Submitted to *Journal of Geophysical Research*, April, 2000.

North-south flows observed in the outer heliosphere at solar minimum: Vortex streets or corotating interaction regions?

M. L. Goldstein, D. A. Roberts, L. F. Burlaga, E. Siregar,[1] and A. E. Deane[2]

NASA Goddard Space Flight Center, Greenbelt, Maryland

Abstract. During the last two solar minima in the distant heliosphere the equatorial heliospheric plasma velocity oscillated perpendicular to the ecliptic plane with an approximately 26-day period in the distant heliosphere. Two explanations have been proposed: compressive interactions between streams and velocity shear interactions that produce a Kármán vortex street. The latter interpretation has been challenged on the basis that the velocity jumps are supersonic, thereby suppressing the Kelvin-Helmholtz (K-H) instability. Here we examine this issue using a time-dependent compressible magnetohydrodynamics code solved in spherical coordinates in the two-dimensional $r - \theta$ plane. We conclude that supersonic flow does suppress small-scale instabilities and that the classic Kármán vortex street cannot be excited. Both velocity shear layers and stream interactions can, however, produce signatures in density, velocity, and magnetic field that resemble the observations. In particular, we find north-south variations of the flow velocity with a period that is approximately half that of the period of the variation in flow speed: a result insensitive to the thickness of the velocity shear layers. A depletion in density (and magnetic field magnitude) relative to the expected Parker value is predicted by the simulations that generate the north-south flow via velocity shear. The Voyager spacecraft observed a similar depletion in the outer heliosphere during the last two solar minima. When the effective tilt of the plasma sheet is increased, corotating interaction regions produce shock waves and other complex time-dependent evolution. We conclude that at solar minimum the observed north-south oscillations are a robust phenomenon that can form from either the interaction of fast and slow solar wind streams or from velocity shear. Which mechanism dominates is a consequence of the degree of tilt of the heliospheric current sheet, the magnitude of the velocity shear, and other physical parameters. However, the depletions seen in density and magnetic flux in the Voyager data suggest that velocity shear in the outer heliosphere at solar minimum may be the dominant cause of the observed north-south flow patterns.

1. Introduction

During solar minimum in 1986, *Lazarus et al.* [1988] reported that data from Voyager 2 collected near 25 AU showed periodic oscillations with a 25.5-day period in the north-south component of solar wind flow velocity. At that time Voyager 2 was near the ecliptic plane. *McNutt* [1988] interpreted the observation of the north-south flow as resulting from pressure gradients at interaction regions produced by compressive effects at corotating streams. This scenario was modeled in a three-dimensional, steady state simulation [*Pizzo*, 1994]. An alternative interpretation [*Burlaga*,

[1] Also at Emergent Information Technologies, Largo, Maryland.

[2] Also at Institute for Physical Science and Technology, University of Maryland, College Park.

1990; *Veselovsky*, 1990; *Veselovsky and Triskova*, 1990] was that the observed north-south flow at solar minimum resulted from a Kármán vortex street that arose as a consequence of the shear between the fast and slow wind near the heliospheric plasma sheet [see also *Triskova et al.*, 1992]. Although the hydrodynamic vortex models [*Burlaga*, 1990; *Veselovsky*, 1990; *Veselovsky and Triskova*, 1990] were suggestive, whether or not the magnetohydrodynamic (MHD) equations would exhibit such solutions if solved for finite amplitude perturbations was not known.

Siregar et al. [1992, 1993, 1994] demonstrated that a vortex street could be excited in Cartesian MHD flows for appropriate parameters. Excitation of a vortex street depends sensitively on the thickness of the separation layer between the two fast flow regions and on the orientation and strength of the background magnetic field. The solutions displayed two maxima per north-south oscillation in the bulk speed, as seen both in the point vortex solution of *Lamb* [1945] and in the Voyager 2 data [*Burlaga*, 1990]. Velocity shears located at the northern and southern boundaries separating fast solar wind (originating from northern and southern polar coronal holes) from slow wind (originating near the heliospheric plasma sheet) could drive a vortex street. Although the solutions presented by *Siregar et al.* [1992, 1993, 1994] agreed qualitatively with the observations, they were insufficiently detailed to make definitive distinctions between the vortex street model and the interaction region model [*Pizzo*, 1994].

Recently, two reports have stimulated renewed interest in this subject. First, *Odstrcil and Pizzo* [1997] pointed out that for supersonic velocity jumps between the fast and slow flows the Kelvin-Helmholtz (K-H) instability is suppressed and excitation of a large-scale vortex street would not be possible [see also *Korzhov et al.*, 1984]. Second, *Burlaga and Richardson* [2000] documented the reappearance in 1995 of periodic oscillations in the north-south component of the solar wind velocity, again near solar minimum, indicating that the 1985 observations were not unique. Such oscillations in the flow velocity are, therefore, a recurring characteristic of the solar wind in the outer heliosphere during solar minimum. The new observations were made when Voyager 2 was near 47 AU at a heliolatitude of $-14.5°$.

In this paper we use a compressible MHD code solved in spherical coordinates in the $r-\theta$ two-dimensional plane to study these north-south flows. For subsonic parameters the K-H instability arises at scales that are initially on the order of the width of the stream-stream boundary and grows to the scale of the separation between the fast and slow streams; both scales are far too small to account for the observations. As noted by *Odstrcil and Pizzo* [1997], the supersonic cases should be stable and not form vortex streets in the traditional sense. The nonlinear solutions, however, can produce north-south oscillations that resemble qualitatively the flow patterns of a true vortex street. In section 2 we describe the algorithm used in the simulations. In section 3 we discuss the previous simulation results. The supersonic case and the role of corotating interaction regions are discussed in section 4. In section 5 we compare the present results to the Voyage 2 observations and include a discussion of some of the limitations of the present model. Our conclusions are summarized in section 6.

2. Numerical Method and Initial Conditions

To study the temporal evolution of velocity shear layers driven by the interaction of northern and southern coronal holes near solar minimum, we solved the inviscid MHD equations in spherical coordinates using a fourth-order flux-corrected transport (FCT) algorithm [*Boris and Book*, 1973; *Zalesak*, 1979; *DeVore*, 1991]. FCT is designed to capture shocks and preserve discontinuities. For a description of the application of this algorithm to the solar wind, see *Goldstein et al.* [1999]. The magnetic field is determined from the electric field using Faraday's law to ensure that $\nabla \cdot \mathbf{B} = 0$ is preserved to within numerical round-off errors. The code advances the density ρ, the momentum $\rho\mathbf{v}$, the total energy (internal (ρe) plus kinetic ($\rho v^2/2$) plus magnetic ($B^2/8\pi$)), and the magnetic field $\mathbf{B}$. The equation of state is that of an ideal gas ($p = \rho RT$), where R is the gas constant and T is temperature.

The MHD equations as solved in the code are

$$\frac{\partial \rho}{\partial t} + \nabla \cdot \rho\mathbf{v} = 0, \tag{1}$$

$$\frac{\partial \rho\mathbf{v}}{\partial t} + \nabla \cdot [(p + \frac{B^2}{8\pi})\mathbf{I} + \rho\mathbf{v}\mathbf{v} - \frac{1}{4\pi}\mathbf{B}\mathbf{B}] = 0, \tag{2}$$

$$\frac{\partial}{\partial t}(\rho e + \frac{1}{2}\rho v^2 + \frac{B^2}{8\pi}) + \nabla \cdot [(\rho e + \frac{1}{2}\rho v^2 + p)\mathbf{v} - \frac{1}{4\pi}(\mathbf{v} \times \mathbf{B}) \times \mathbf{B}] = 0, \tag{3}$$

$$\frac{d\mathbf{B}}{dt} = -c\nabla \times \mathbf{E}, \tag{4}$$

where

$$\mathbf{E} = -\frac{1}{c}\mathbf{v} \times \mathbf{B}, \tag{5}$$

together with the relation

$$p = (\gamma - 1)\rho e. \tag{6}$$

Here $\mathbf{I}$ is the unit tensor with components δ_{ij} and γ is the ratio of specific heats. In the results discussed in section 3,

$\gamma = 3/2$ [*Siscoe and Intriligator*, 1993; *Totten et al.*, 1995]. In regimes of low plasma beta ($\beta = 8\pi p/B^2 \ll 1$), the thermal pressure can become negative because of the tendency of the plasma to cavitate when β is low and γ is high. To avoid this numerical artifact, we have implemented a technique (P. Cargill, private communication, 2000) that takes advantage of the fact that when entropy is conserved, the energy equation can be written in conservative form as

$$\frac{\partial p^{1/\gamma}}{\partial t} + \nabla \cdot (\mathbf{v} p^{1/\gamma}) = 0. \tag{7}$$

Following *Cargill et al.* [2000], we compare the pressure computed from (3) to that computed from (7). When the former is less than the latter, we use the solution of (7) and recompute the internal energy using p as determined from (7). In regions that have been shocked, p computed from (3) is always larger than p computed from (7). Consequently, the solution of (3) is always used where nonadiabatic heating has occurred.

Because the primary effect we are exploring arises at solar minimum when the azimuthal structure is slowly varying, we could limit the domain of integration to a wedge of latitudinal extent $\Delta\theta$ in the $r - \theta$ plane. Fast flow occupied the northern and southern portions of the wedge, while slow flow occupied the central portion. To simulate the interaction between the two fast flow regions, we drove the radial velocity at the shear layers at a low frequency corresponding to the solar rotation rate. The shear layers, which were made to oscillate slightly in θ at the same low frequency, then bounded a region of slow flow containing an equatorial current sheet. The Archimedian spiral field [*Parker*, 1963] was included by adding a constant $B_{\phi 0}$ at the inflow boundary. Because $B_r(r) \sim 1/r^2$, B_ϕ ($\sim 1/r$) becomes increasingly dominant at large r, and a global spiral pattern results. In these runs, $B_{\phi 0} = {}^1\!/_3 B_r(r = r_0)$, where r_0 is the inflow boundary. The ϕ component of the spiral field rotates through the current sheet so that it is positive in the south and negative in the north. The separation of the two velocity shear boundaries was a parameter that could be varied to ensure that at small separation the two velocity shears could interact [cf. *Siregar et al.*, 1992, 1993, 1994].

The θ variation in radial velocity was given by:

$$\begin{aligned} v_r(\theta) = v_0 & \\ & + \frac{\delta v_\parallel}{2} \tanh\left[\frac{\Theta_-}{\Delta}\right] \tanh\left[\frac{\Theta_+}{\Delta}\right] \\ & + \delta v_r \sin(\Omega t) \left\{ \exp\left[-\left|\frac{\Theta_-}{\Delta}\right|\right] - \exp\left[-\left|\frac{\Theta_+}{\Delta}\right|\right] \right\}, \end{aligned} \tag{8}$$

for

$$\frac{\pi - \theta_0}{2} \le \theta \le \frac{\pi + \theta_0}{2}.$$

The thickness of the shear layer is $\Delta \ll \theta_0$, $\Theta_\pm = \theta - \delta v_\theta \sin(\Omega t) - (f_w \pm 1)(\pi - \theta_0)/(2 f_w)$, and Ω represents the 25.5-day solar rotation. The parameter $1/f_w$ is the fraction of the θ domain filled by slow flow. The velocities v_M and v_m are the fast and slow flows at the inflow boundary, respectively. In addition, $\delta v_\parallel = v_M - v_m$, and $v_0 = (v_M + v_m)/2$. For $\Omega = 0$, (2) produces fast flow at high and low latitudes and slow flow within a narrow wedge centered at the equator. For $\Omega \neq 0$ the shear layers oscillate in latitude at a frequency Ω and amplitude δv_θ. An additional asymmetric perturbation in radial velocity with amplitude δv_r is centered at the shear layers to simulate small speed differences between the two fast streams.

The flow into the volume at $r = r_0$ is both super-Alfvénic and supersonic with Alfvénic and sonic Mach numbers M_A and M_s, respectively. The flow remains supersonic and super-Alfvénic to the outflow boundary at $r = r_{\max}$. Linear extrapolation outflow boundary conditions were used at the wedge boundaries at $\theta = 1/2(\pi \pm \theta_0)$ and at $r = r_{\max}$. The radial magnetic field was initialized with $B_r(r, \theta, t = 0) = B_{r0}(\theta)(r_0/r)^2$. The radial density profile at $t = 0$ was defined using an approximation to Parker's asymptotic solution [*Parker*, 1963] with $\rho_0(r = r_0, t = 0) = 1/4\pi$. Setting $\rho_0 = 1/4\pi$ effectively renormalized the magnetic field to Alfvén speed units. Consequently, at $t = 0$ the Alfvén speed at the inflow boundary was $V_A = B_{r0}$. Temperature T is not a dynamical variable, but can be determined from the thermal pressure p and the equation of state. For the simulations discussed in sections 3 and 4 we take T to be uniform on the inflow boundary.

A current sheet was placed at the equator at $\theta = \pi/2$, and the pressure was initialized so that the fluid and magnetic field were in approximate pressure balance. The oscillation of the velocity shear layers, which models the rotation of a tilted plasma sheet, required that $B_r(r, \theta, t)$ also oscillate. In analogy to (2), this was accomplished using a $\tanh$ function with a time-dependent argument and angular amplitude of oscillation δv_θ, so that

$$B_r(r_0, \theta, t) = B_{r0} \left[\tanh\left(\frac{\Theta}{\Delta}\right)\right] \tag{9}$$

in the θ domain of integration (with $\Theta = \theta - \delta v_\theta \sin(\Omega t) - (\pi - \theta_0)/2)$). To model the heliospheric current sheet, we rotated the magnetic field in azimuth across the current sheet by π radians to approximate the reversal of the field. The oscillation of the velocity shear layers introduced a similar

time dependence into $B_{\phi 0}$, so that

$$B_{\phi 0}(r_0, \theta, t) = B_{\phi 0}\left[\tanh\left(\frac{\Theta}{\Delta}\right) - \frac{1}{b_c \cosh\Theta}\right], \quad (10)$$

where $b_c = 1/3$ in the runs described below. The first term in (10) introduces the ϕ component of the Parker field, and the second yields a rotation rather a reversal.

The time-dependent boundary condition on $B_r(\theta)$ necessitated that a similar time dependence be defined for $v_\theta(0, \theta, t)$ to preserve frozen-in flow. All the solutions discussed in sections 3 and 4 were computed on an $r - \theta$ mesh of 512×128 points. The units of length and time were taken to be unity, which, together with $\rho_0 = 1/4\pi$, effectively normalized all the variables to dimensionless units. The parameters used for the four runs described in this paper are summarized in Table 1.

3. Comparison With Earlier Simulations

Our previous studies of the observed north-south flow oscillations used either the Chebyshev-Fourier method to solve the resistive, compressible MHD equations in two Cartesian dimensions on a 64^2 mesh [*Siregar et al.*, 1992, 1993] or a Galerkin spectral algorithm to solve the resistive incompressible MHD equations in three dimensions [*Siregar et al.*, 1994] on a 64^3 mesh. The strength of the interaction between the two velocity shear layers was determined by the ratio S of the initial distance between the vortex sheets to the perturbation wavelength. The two layers interacted only for sufficiently small S. The Reynolds number R_m used in the Chebyshev-Fourier method was the maximum consistent with the number of modes in the simulation and the requirement that energy not accumulate at the dissipation scale. A typical value was $R_m = 10^3$ in the two-dimensional study and $R_m = 500$ in the three-dimensional study.

Given the limited resolution of the earlier calculations [*Siregar et al.*, 1992, 1993, 1994], the dissipation scale was only slightly smaller than the width of the velocity shear layers. Because the observed north-south oscillations occur at large radial distance (21 AU in 1986 and 47 AU in 1995), the fact that the earlier studies solved the MHD equations in Cartesian, rather than spherical, coordinates was unimportant. Despite the relatively small sizes of the previous simulations, *Siregar et al.* [1992, 1993, 1994] demonstrated that the flow could become unstable and that antisymmetric perturbations could grow to form a vortex street. Their solution contained the essential observational feature that the average flow velocity had two maxima for each north-south oscillation. The three-dimensional results [*Siregar et al.*, 1994] suggested that a fairly strong background magnetic field parallel to the axis of the vortices was essential to preserve a coherent vortex tube. Weak background magnetic fields would allow the vortices to kink. In addition, if the magnetic field were not oriented essentially orthogonal to the solar wind velocity, the K-H instability would be suppressed [*Parker*, 1964; *Korzhov et al.*, 1984]. The observed magnetic fields in the outer heliosphere do, however, appear to be sufficient to organize any vortex tubes [see, e.g. *Roberts et al.*, 1990].

None of these previous studies investigated the role of the sonic Mach number. In the two-dimensional compressible calculations, the velocity jumps across the shear layers were subsonic, while the three-dimensional simulation was incompressible and thus implicitly subsonic.

3.1. An Unstable Solution: Formation of a Kármán Vortex Street

To illustrate the importance of Mach number and other parameters on the development of a Kármán vortex street, run A (Table 1) was designed to satisfy the K-H instability criterion $v_M - v_m < 2\sqrt{2}C_s$. The situation was nearly Cartesian; the length of the system was 30, and $r_0 = 40$, in dimensionless units. The Mach number was $M_s = 2$, and the initial flow speed was $v_0 = 0.714$. At the inflow boundary the difference between the speed in the fast and slow flows was $v_M - v_m = 0.21$, and $C_s = 0.35$; thus $2\sqrt{2}C_s = 0.98$. For this run, $\theta_0 = 3°$, the initial shear layer thickness was $\Delta \approx 0.05°$, $M_A = 50$, and slow flow occupied the central $1/4$ of the latitudinal domain. Making the slow flow region narrow and the shear layers thin was critical for the excitation of the resulting vortex pattern. The subsonic instability is difficult to excite; its growth is sensitive to the parameters chosen, especially the rate of expansion, which must be small, and the width of the velocity shear layers and slow flow region, both of which must be narrow.

In Figure 1 we show a gray scale image of the magnitude of the vorticity ω, muliplied by r^2 for this subsonic situation. The large-scale long-wavelength oscillation represents the forcing of the fast streams from the northern and southern hemispheres. As the fluid convects into the domain of integration the two shear layers begin to interact, producing vortices. The pattern, however, resembles neither the point vortex solutions described by *Burlaga* [1990] and *Veselovsky* [1990] nor the observations. The scale of the vortex pattern is determined by the separation of the shear layers and by their thickness, not by the forcing function. Thus the scales of the north-south flows are unrelated to the simulated rotation rate. Furthermore, no interaction regions form, and consequently, such K-H unstable simulations cannot generate observables such as deficits in the density and correlations or lack thereof between density and magnetic field magnitude.

Table 1. Summary of the Parameters Used in the Simulations

Run	δv_θ, deg	r_0	$r_{\max}$	θ_0, deg	Δ, deg	f_w	M_s	M_A	$M_s \frac{\delta v_\parallel}{v_0}$
A – subsonic	≈ 0.1	40	70	3	0.05	4	2	50	1.2
B – supersonic	≈ 4.0	10	130	45	2	4	6	5	2.4
C – supersonic	≈ 0.4	10	130	24	1	8	6	5	2.4
D – supersonic	≈ 1.0	10	130	24	1	3	6	5	2.4

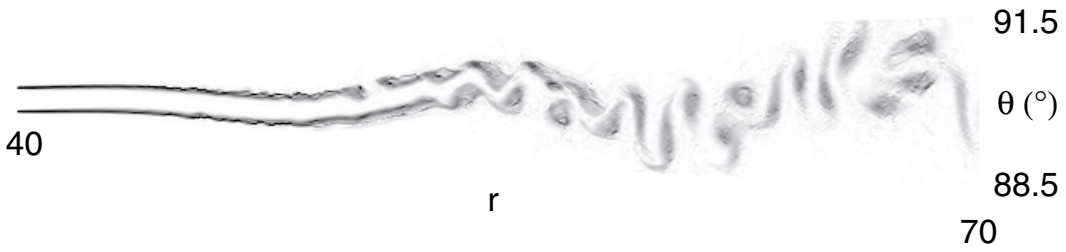

Figure 1. A gray scale image of the normalized vorticity (ωr^2) for a K-H unstable simulation (run A) of a velocity shear instability with two velocity shear layers.

3.2. Role of Compressive Interaction Regions

The second case we investigate is similar to that suggested by *McNutt* [1988], *Pizzo* [1994], and *Pizzo et al.* [1995]. *Pizzo* [1994] and *Pizzo et al.* [1995] used a three-dimensional solution of the time-independent MHD equations to investigate the north-south flow phenomenon. In contrast, the case described here is time-dependent, but two-dimensional. The run (run B in Table 1) has a relatively wide latitudinal domain ($\theta_0 = 45°$) and a north-south amplitude of oscillation ($\delta v_\theta \approx 4°$). In this case, slow flow occupies the central $1/4$ of the latitudinal domain. The Mach numbers M_s and M_A were 6 and 5, respectively, and the initial mean flow speed was $v_0 = 0.714$. At the inflow boundary, $v_M - v_m = 0.285$, and $C_s = 0.119$, so that the velocity jump is supersonic, and although $v_M - v_m$ is just a little smaller than $2\sqrt{2}C_s$, the growth rate is too small to be important (we have run cases with $v_M - v_m > 2\sqrt{2}C_s$ and found identical behavior). In this and subsequent runs, $r_0 = 10$, and $r_{\max} = 130$.

The resulting flow pattern is illustrated in Figure 2, which shows contours of B together with a gray scale image of ωr^2. The thickness of the shear layer is $\Delta \approx 2°$. The sharp gradients in B are associated with shock waves that have formed as the corotating interaction regions compress. Figure 3, a gray scale image of ρr^2 and the same contours of B, shows the compressions, rarefactions, and shock waves more clearly.

A velocity-field vector plot for run B (Figure 4) shows

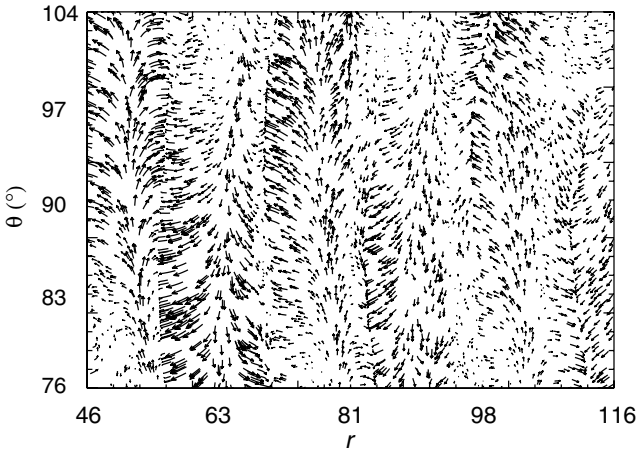

Figure 4. A velocity field plot from run B.

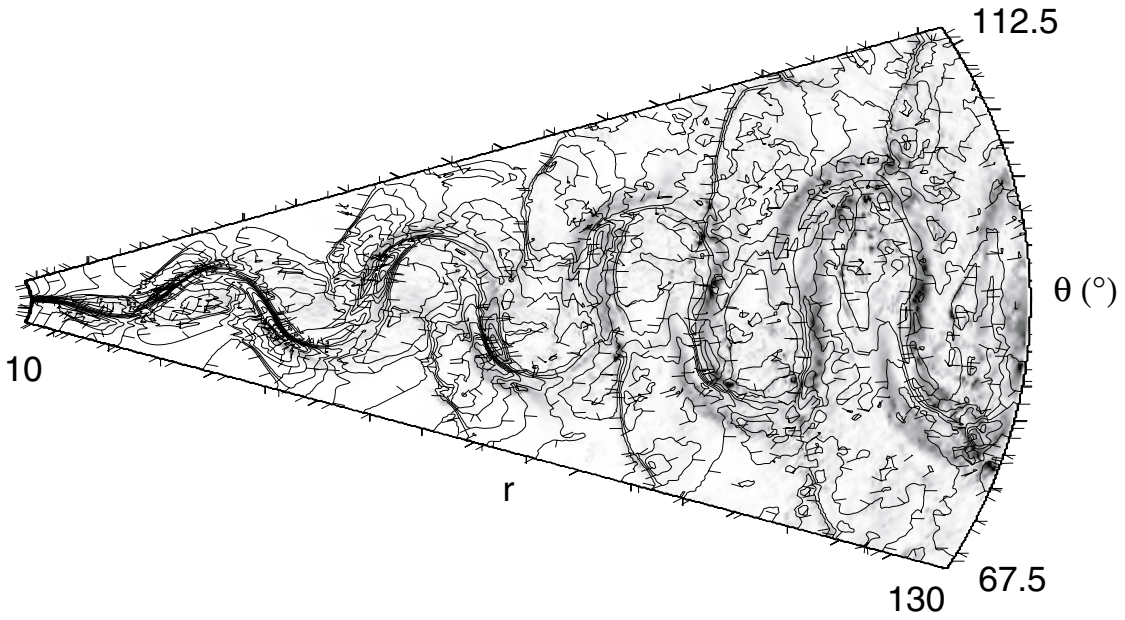

Figure 2. Contours of magnetic field magnitude B superimposed on a gray scale image of normalized vorticity (ωr^2) from a simulation designed to produce interaction regions. The slow flow occupies $1/4$ of the latitudinal domain (run B). The tick marks on the contours in this and Figures 3, 6, 10, 12, and 13 indicate the "downhill" direction.

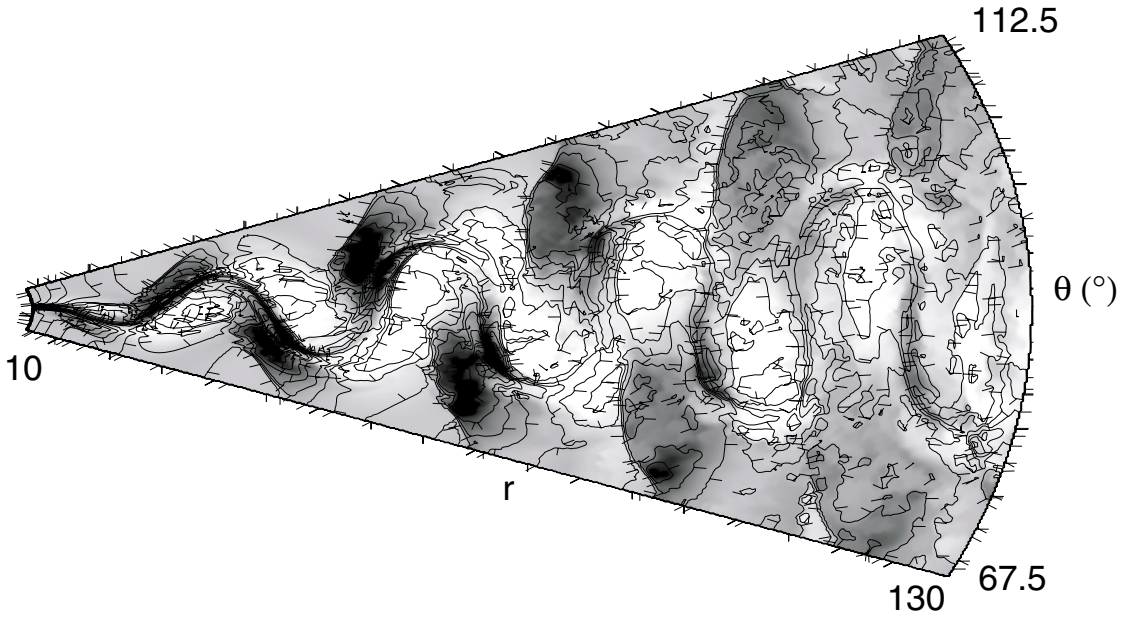

Figure 3. Contours of B superimposed on gray scale contours of ρr^2 from run B.

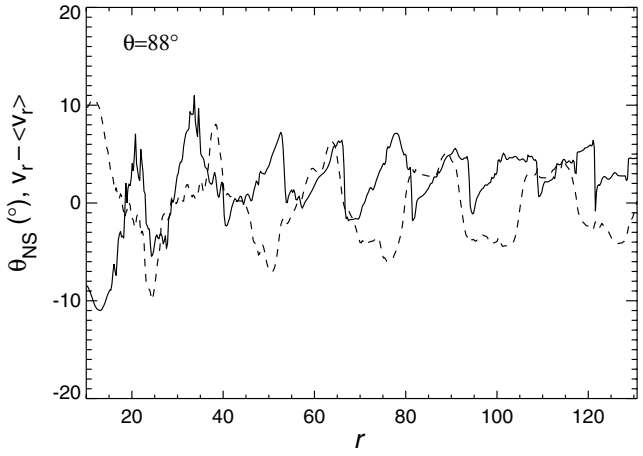

Figure 5. (a) Plots of θ_{NS} (dashed line) and $(v_r - < v_r >)$ (solid line) from run B (Figures 2 and 3). The data sample is from $\theta \approx 82°$.

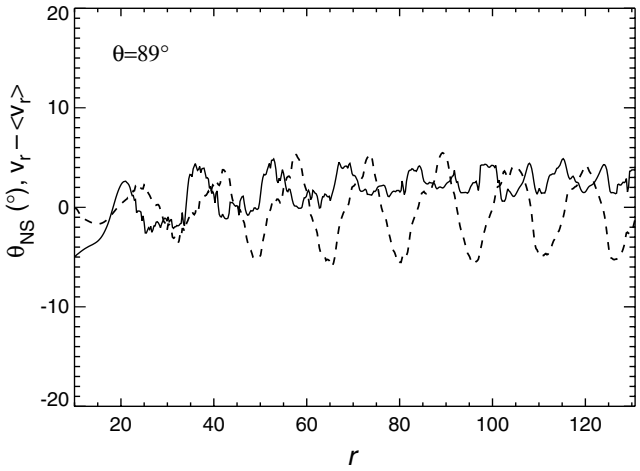

Figure 7. Plots of θ_{NS} (dashed line) and $(v_r - < v_r >)$ (solid line) from run C (Figure 6). The data sample is from close to the equator at $\theta \approx 89°$.

that while strong vortical motions are present, they are not well organized with respect to the equator and are dominated by strong north-south flows; the apparent discontinuities evident in the vector directions reflect the presence of shock waves. The combination of the $4°$ amplitude of the forcing function δv_θ and the strong shock waves produces the north-south oscillations of $\theta_{NS} \equiv \tan^{-1}(v_\theta / v_r)$ and $v_r - < v_r >$ shown in Figure 5 (θ_{NS} and $v_r - < v_r >$ are plotted as the dashed and solid curves, respectively). The cut is taken at $\theta \approx 88°$. The north-south oscillation patterns and periodicities seen in the steady state solutions [*Pizzo*, 1994] are present, but with a great deal of structure, reflecting the time dependence and the very small dissipation characteristic of the FCT algorithm. The pattern becomes more complex at higher latitudes, and eventually, θ_{NS} and v_r have the same periodicity. The strong compressions produced from the interaction of the fast and slow flows produced high correlations between ρ and B throughout the radial domain.

4. Role of Velocity Shear in Supersonic Flow

Although the strong compressive interaction regions reproduce many features of the observations, in this section we explore the extent to which velocity shear in the absence of strong interaction regions can also account for the Voyager 2 observations. The relevant runs (runs C and D in Table 1) have supersonic jumps in velocity with $C_s = 0.119$ with $v_0 = 0.714$ and $v_M - v_m = 0.285$, as in run B. The velocity shear layers had a latitudinal width of $\Delta \approx 1°$, and the total wedge in latitude was $\theta_0 = 24°$, still consistent with observations. For run C, the central $1/8$ of the domain contained slow fluid; this was increased to $1/3$ for run D to investigate the role of the width of the slow flow region.

Figure 6 shows a gray scale image of ωr^2 for run C together with contours of B. As expected, the vortical regions do not exhibit the classical roll-up characteristic of a K-H instability or Kármán vortex street. However, a prominent feature of the observations is that the bulk speed exhibits two maxima per north-south oscillation (Figure 7, where θ_{NS} and v_r are plotted as the dashed and solid curves, respectively). The output is from $\theta \approx 89°$, close to the equator. The two-maximum pattern is present much of the time.

In the Voyager 2 observations [*Burlaga and Richardson*, 2000], the two maximum pattern is not always present, especially during 1995. In runs C and D, as in run B, the pattern disappears as one moves away from the equatorial plane and is no longer present at $\theta = 87°$. The magnitude of the north-south oscillation shown in Figure 7 ($\delta\theta_{NS} \approx \pm 6°$) is close to that reported ($\approx \pm 4°$) [*Burlaga and Richardson*, 2000]. We do not see the pronounced decrease in the oscillations with distance found by *Pizzo* [1994]. That decrease may have been a consequence of numerical diffusion, although A. Usmanov (private communication, 2000) points out that the falloff of the oscillations with distance in the *Pizzo* [1994] calculations appears to increase with increasing tilt angle of the dipole. During the two time periods of the Voyager observations the tilt was small, so the apparent discrepancy with the observations that we find with the *Pizzo* [1994] calculation may not arise for small tilt angles. For comparison with runs C and D we show in Figure 8 the 1986 data from *Burlaga and Richardson* [2000]. In Figure 9 we show a plot of the velocity vectors from $46 < r < 116$ and $83° < \theta < 97°$ from run C. The rotation of the fluid in

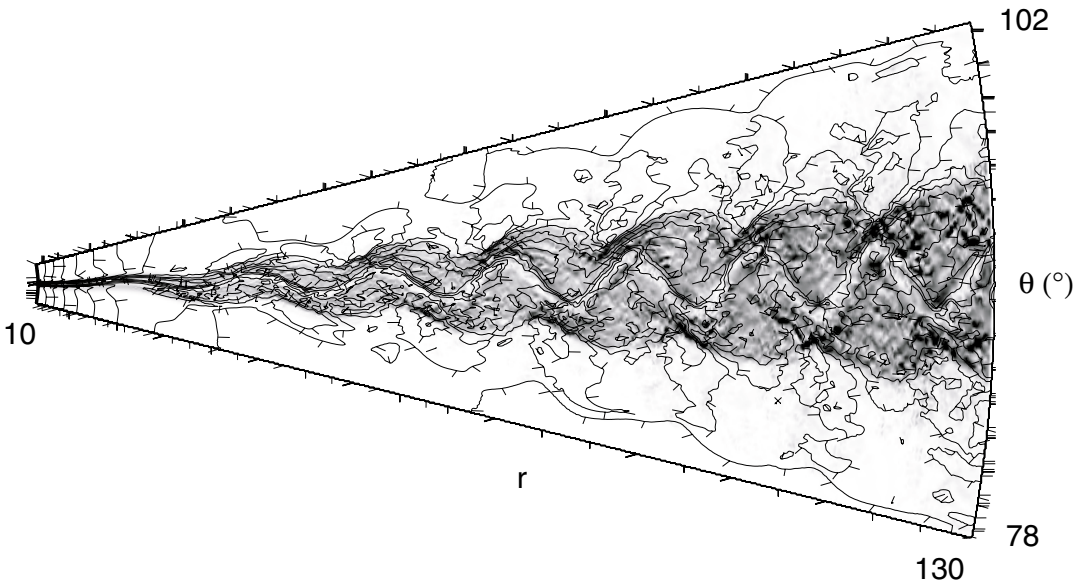

Figure 6. Contours of magnetic field magnitude B superimposed on gray scale contours of normalized vorticity (ωr^2) from run C.

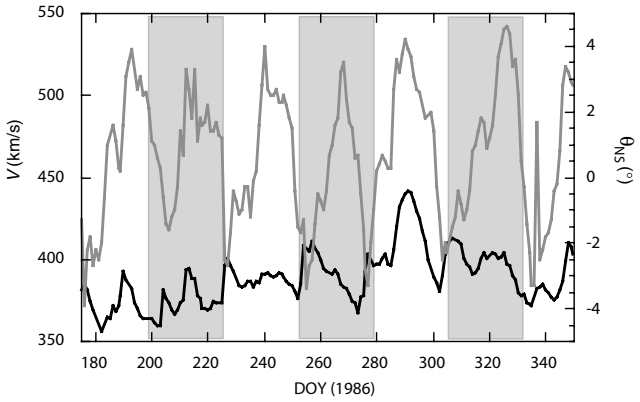

Figure 8. Data from Voyager 2 in 1986. The upper curve is θ_{NS}, and the lower curve is the solar wind speed. The shaded regions span approximately 25 days. During much of the time period the speed shows two peaks for each 25-day period.

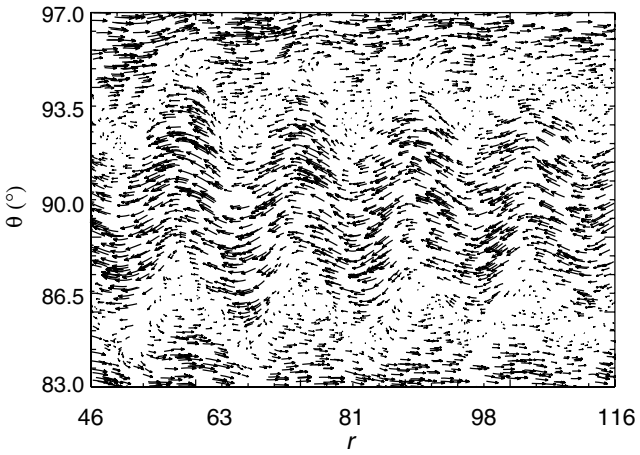

Figure 9. A velocity field plot showing the tendency for vortical motion in the rest frame of a flow with supersonic flow velocity jumps between the fast and slow flows (run C).

the rest frame of the bulk flow shows a very clear alternating pattern north and south of the equatorial slow flow region, not unlike the pattern formed by a true vortex street.

When north-south flows were observed in 1986, *Burlaga and Ness* [1993] noted that near the heliospheric current sheet the magnetic flux was systematically low with respect to the expected Parker value. The deficit was not present

at other times [*Burlaga and Ness*, 1993, cf. Figure 4] and thus was not the same phenomenon as the controversial observations of a pervasive flux deficit near the heliospheric equator reported by *Slavin et al.* [1984] and *Winterhalter and Smith* [1989]. *Pizzo and Goldstein* [1987] tried to model the observed flux deficits, and their axisymmetric model with a tilted dipole is quite similar in conception to the situation modeled in runs C and D. However, Pizzo and Goldstein's paper predated the observations of the north-south flows, and the possiblity of such flows was not discussed. For numerical reasons the *Pizzo and Goldstein* [1987] calculations for nonaxisymmetric flows were confined to tilt angles larger than 10° and therefore are not directly relevant to heliospheric conditions when the north-south flows and flux deficits were observed. [*Pizzo and Goldstein*, 1987, p. 7251] point out that "internally generated meridional transport ... should be most prominent during the late declining and near-minimum phases of the solar cycle, when the coronal geometry is most regular and least complicated." That is precisely the time period that the flux (and density) deficits were observed as well as being the conditions that runs C and D were designed to model. Both the conditions in the heliosphere and runs C and D reflect conditions that minimize compressive effects associated with strong fast/slow stream interactions.

In association with the flux deficit, *Burlaga and Ness* [1993] reported a decrease of $\sim 10\%$ in the solar wind speed relative to the speed both before 1986 and after 1987. The rotating flows (in the rest frame of the bulk flow) in the simulation expel magnetic flux from regions of slow flow, consistent with the Voyager 2 observations (compare Figure 6 and *Siregar et al.* [1993]). The vortical motion produces local values of v_r that are either smaller or larger than the mean, depending on one's location in latitude. Locations close to the equator, in the slow flow region, will preferentially flow more slowly than the mean (compare Figure 9).

In addition to the relatively weak expulsion of magnetic flux (Figure 6), the flux depletion regions are associated with density depressions. In Figure 10, contours of B are superimposed on a gray scale image of ρr^2, and a generally positive correlation between B and ρ is apparent. The correlation is also evident in cuts taken along lines of constant latitude. Figure 11 shows a cut near the center of the slow flow region ($\theta \approx 90^\circ$). As indicated by the shaded area, there are places in the simulation domain where the correlation disappears. At higher latitudes the correlation becomes more positive as the morphology of flow becomes increasingly determined by the compressions induced by the interaction regions. Also evident in Figure 10 is that near the inflow, ρ is high at the center of the plasma sheet, as expected in slow solar wind, and is less dense at high and low latitudes in the

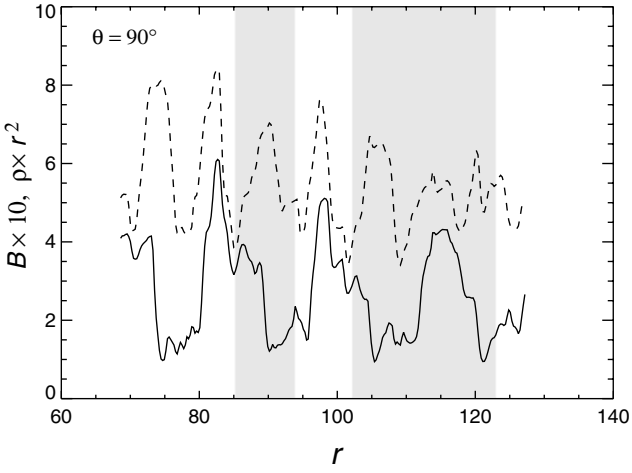

Figure 11. Plots of $B \times 10$ (solid line) and ρr^2 (dashed line) from the contours shown in Figure 10. The data have been sampled close to the center of the slow flow region at $\theta \approx 90^\circ$.

faster-flowing fluid. As the radial distance increases, however, the plasma sheet near the equator becomes underdense relative to the r^{-2} normalization. Underdense, slowly flowing plasma is observed in the outer heliosphere at the time the north-south flows were present [*Richardson et al.*, 1999]. This pattern will have an approximately 26-day periodicity because near the maximal excursions of the current sheet the fluid is compressed and the density is higher than it is near the equator (compare Figures 10 and 13). We return to this point in section 5.

In contrast to the situation in subsonic flows, we found that the signatures of velocity shears in supersonic flows are relatively insensitive to particular choices made for the thickness of the velocity shear layers and the width of the slow flow regions. We show one example from a simulation that was run in which slow flow occupied a wedge of $1/3$ of the latitudinal computational domain of $\theta_0 = 24^\circ$ (run D in Table 1). The width of the velocity shear layers in this case was 1°. Contour plots of ωr^2 and B are shown in Figure 12, and in Figure 13 the gray scale image of ρr^2 and contours of B highlight the nature of the interaction regions that form in this case. In the rest frame of the bulk flow, the velocity vectors rotate in a manner similar to that seen previously in Figure 9 and are not plotted here. For the parameters of run D the north-south oscillation pattern is very clearly defined (compare Figure 14 and the Voyager observations, Figure 8) with the flow speed v_r having a periodicity that is half that of θ_{NS}. Run D also produced high correlations between ρ and B that we have not plotted.

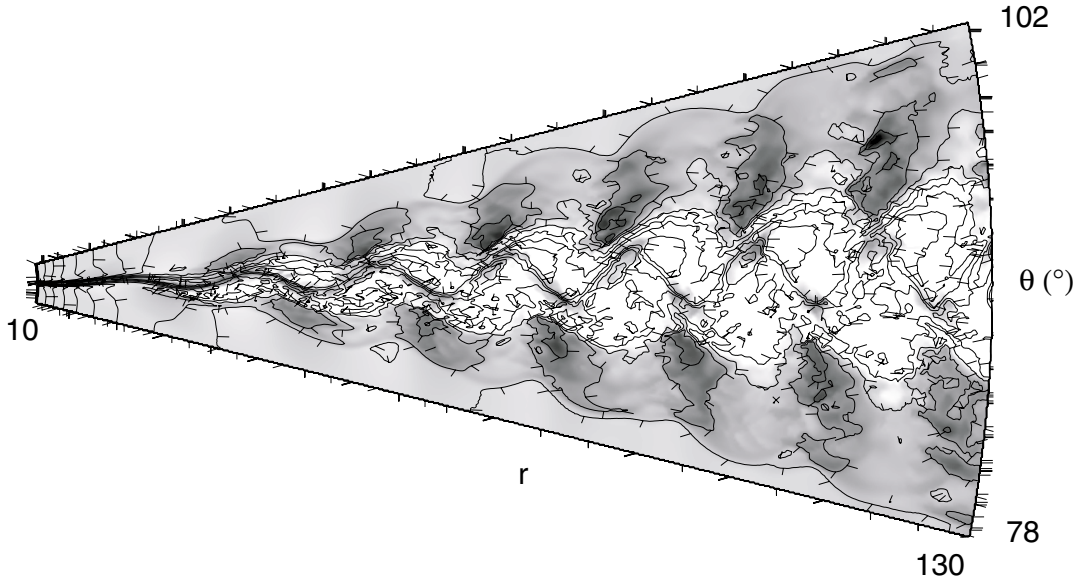

Figure 10. Contours of magnetic field magnitude B superimposed on gray scale contours of ρr^2 for run C.

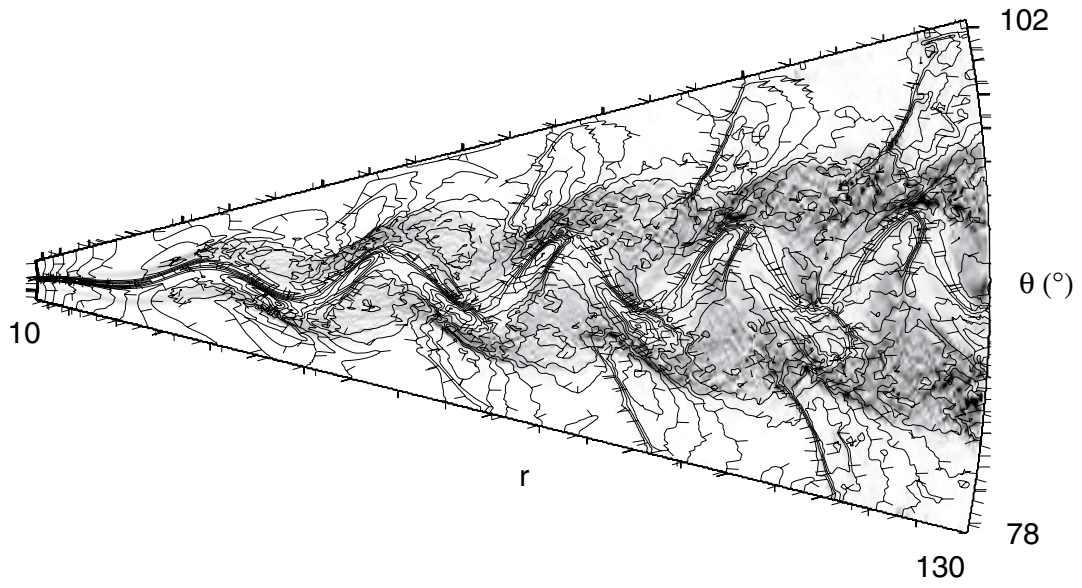

Figure 12. Contours of magnetic field magnitude B superimposed on gray scale contours of normalized vorticity (ωr^2) from a simulation initiated with broad velocity shear layers and slow flow that occupied $1/3$ of the latitudinal domain (run D).

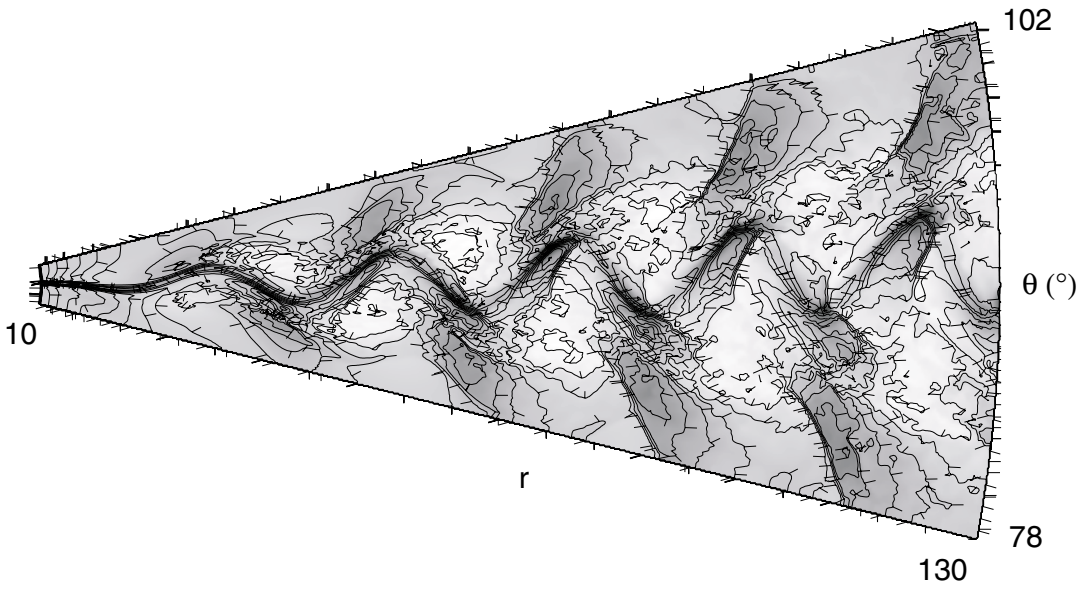

Figure 13. Contours of B superimposed on gray scale contours of ρr^2 from run D.

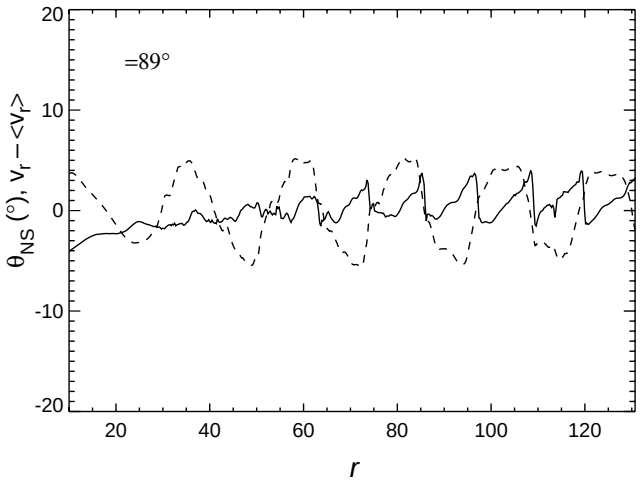

Figure 14. Plot of θ_{NS} (dashed line) and $(v_r - < v_r >)$ (solid line) from the wide supersonic simulation (run D) shown in Figures 12 and 13. The data sample is from close to the equator at $\theta \approx 89°$.

5. Discussion

We have designed a series of simulations to model the Voyager 2 observations of a strong north-south oscillation of solar wind velocity in the outer heliosphere during the past two minima in solar activity. In the simulations, the oscillation of the north-south angle of the flow velocity θ_{NS} has a scale length determined by the frequency of the forcing function imposed to simulate the rotation of a tilted heliospheric current sheet. In the first simulation, the velocity jumps between the fast and slow regimes satisfied the K-H instability criterion, which resulted in vortical flows that did not have the observed heliospheric pattern. Finding parameters that would excite this "vortex street" was difficult; both the velocity shear layers and the region of slow flow had to be narrow, and the flow geometry had to be nearly Cartesian. While the nearly Cartesian situation does approximate the situation in the outer heliosphere at solar minimum, that appears to be the only feature of the subsonic velocity jump regime that resembles the observations. Thus the observations are not indicative of excitation of a Kármán vortex street in the classical sense.

Both our simulations and those of [*Pizzo*, 1982, 1994], and [*Pizzo et al.*, 1995] are highly idealized representations of the heliosphere, albeit in different ways. While the *Pizzo* [1982, 1994] and *Pizzo et al.* [1995] computations were three dimensional, the resolution was, of necessity, modest, the equations solved were time-independent, and the algorithm

employed had more numerical dissipation than the FCT algorithm used here. Our results, while two dimensional, have high spatial resolution in those two dimensions, and are time-dependent. Furthermore, the FCT algorithm was designed to preserve fine-scale spatial and temporal structure with minimal numerical dissipation or diffusion. The evolution of interacting Alfvén and slow- and fast-mode waves cannot be described in a steady state model which assumes that all characteristic disturbances propagate at the fast-mode speed perpendicular to the magnetic field. The apparent discrepancies in how interaction regions evolve and what flow patterns accompany them between these two groups of simulations require further investigation in three dimensions, especially with regard to the role of the tilt angle of the solar magnetic dipole. Time-dependent effects become increasingly important as one models phenomena at large heliocentric distances. Such studies are computationally expensive, in part because time-dependent initial conditions must be prescribed at fairly small radial distances if one is to compute accurately the flow patterns at large distance.

In runs C and D with supersonic velocity jumps between the fast and slow flows but with a smaller degree of tilt of the plasma sheet than in run B, large and coherent oscillations in the flow speed formed. Near the equator the magnitude of the flow speed generally showed two peaks in v_r for each cycle of θ_{NS} (compare Figure 7). The magnitude of the oscillations in θ_{NS} ($\approx \pm 5^\circ$) is similar to those observed [*Lazarus et al.*, 1988; *Burlaga and Richardson*, 2000]. In the supersonic regime, the north-south flow pattern appeared to be a very robust result, relatively insensitive to the detailed structure of the plasma sheet or velocity shear layer. However, the pattern of two peaks in v_r for each cycle of θ_{NS} disappeared more rapidly with latitude in runs C and D than in run B, where the pattern was still recognizable even at 70°, albeit distorted by the shock waves and other small-scale stationary and evolving structures.

Another feature of runs C and D is that the normal density pattern that is observed in the inner heliosphere is inverted at large radial distances. In the inner heliosphere and at small r in the simulations, ρ is larger in the plasma sheet than it is in the faster-flowing fluid, primarily because of pressure balance arising from the fact that the magnetic field in the slow flow region, which contains a current sheet, is weaker than it is at higher latitudes. Thus the density must be higher in the slow flow. However, at larger r the simulations show that ρ becomes lower in the slow flow regime than it is in the fast flow. The pattern is correlated with the deficit in magnetic flux and with the reduction in v_r that results near the equator due to the vortical flow. A search of summary records of density over the past two solar cycles revealed that a reduction in the solar wind density with respect to the r^{-2} extrapolation from 1 AU IMP 8 data was present in 1986 and 1995 on Voyager 2 [see, e.g. *Richardson et al.*, 1999]. Indeed, as pointed out by [*Pizzo and Goldstein*, 1987, p. 7251], "at the low dipole tilt angles typical of solar minimum the very distinction between [stream-induced transport and axisymmetric velocity shear in producing flux deficits] becomes philosophical." Nonetheless, it is important to emphasize that velocity shear itself, when perturbed by forcing generated by a rotating tilted dipole, will generate large-scale eddies that naturally give rise to the observed north-south flows. Although meridional transport and north-south flows will arise from compressive stream-stream interactions, such interactions are not required.

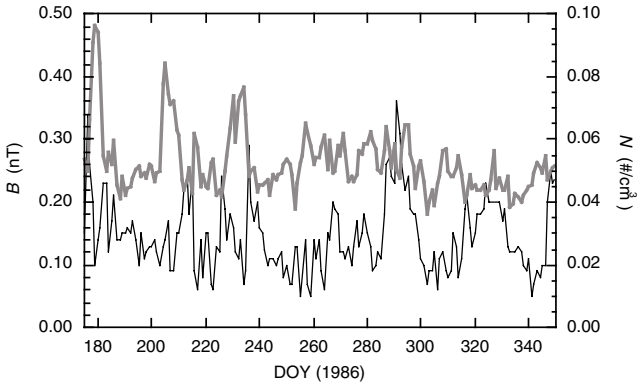

Figure 15. Voyager 2 data from 1986 showing both B (thin solid line) and ρ (thick solid line) during the period of time that a vortex street may have been present.

In the supersonic simulations, the interaction regions generate positive correlations between B and ρ throughout some, but not all, of the radial domain. Positive $B-\rho$ correlations are generally not observed, although periodic peaks in the total pressure are observed [*Lazarus et al.*, 1988]. In Figure 15 we have replotted the data for 1986 for both B and density N from *Burlaga and Richardson* [2000] (the magnetic field for the 1995 epoch was too weak to be included in the *Burlaga and Richardson* [2000] analysis). The temperature T (not plotted), which contributes significantly to the total pressure, is somewhat better correlated with B than is N. The observed correlation between B and N is generally weak, except that during the beginning of the data interval the density shows strong peaks suggesting that one or two interaction regions might be present. Even during that period, however, the magnetic field shows little positive correlation with either N or T [see *Burlaga and Richardson*, 2000]. During the 1986 interval, and also during 1995, the density suggests that no interaction regions were present. In fact, beyond about 20 AU, interaction regions and the sector pattern itself tend to disappear [*Burlaga et al.*, 1997], per-

haps because interstellar pickup ions are becoming assimilated into the solar wind. These particles have high effective temperatures and pressures and will tend to broaden and damp the interaction regions. Although it should be possible to include this effect within the context of a more general multifluid MHD model, doing so is beyond the scope of the present study except to note that one might consider the pickup ions primarily to constitute an additional pressure whose effect could be approximated by a larger value of γ.

6. Conclusions

Because the velocity contrast between fast and slow flow in the outer heliosphere is almost certainly supersonic, the classic vortex street cannot form. Nonetheless, as illustrated in runs B, C, and D, both the velocity shear and interaction regions can reproduce the observation that θ_{NS} has half the period of the oscillation in v_r. The observed depletions in both B and ρ in the outer heliosphere at solar minimum, however, suggest that velocity shear plays an important role in determining both the observed north-south flow patterns as well as the observed flux and density deficits. This behavior is reminiscent of the results of the axisymmetric calculations of *Pizzo and Goldstein* [1987], although they did not investigate the periodicity of meridional flows. The meridional motions we find in the absence of strong stream interactions do not sweep the magnetic flux and plasma density to high latitudes; rather, the flux and density are swept away from the equator in a manner not dissimilar to that pictured by *Burlaga* [1990, Figure 1]. Strong interactions between fast and slow flows, enhanced by large dipole tilt angles, cannot as readily account for either the density depletions or the flux deficit in B. Further research is needed with time-dependent three-dimensional simulations to clarify the relative importance of those two drivers.

We have shown that flows that produce strong north-south oscillations will arise even when the jump in velocity across shear layers is supersonic and the classic Kelvin-Helmholtz instability is suppressed. Our numerical simulations were two-dimensional solutions of the time-dependent ideal compressible MHD equations. Nonideal behavior arises from the residual numerical dissipation present in the algorithm. The vortex-street-like behavior is driven by a forcing function that models the alternating fast solar wind that originates from the northern and southern coronal holes at solar minimum as a tilted plasma sheet rotates. The presence of two velocity shear interfaces will generate oscillations that produce north-south flows. The process is not an instability because the final state is not determined by the fluid parameters, but by the magnitude of the imposed forcing function. The suppression of the K-H instability is a virtue in this picture, for otherwise the most unstable mode would have a very short wavelength determined by either the dissipation scales or shear scales in the system.

Whether or not the double-peaked structure of θ_{NS} with respect to each period of v_r appears depends on the latitude at which the velocity is sampled and on the amplitude of the forcing (δv_θ). The north-south oscillations are a fairly robust result; broad velocity shear layers or thick regions of slow flow tend to affect the magnitude of the oscillations but not the qualitative behavior.

In runs C and D, which have small dipole tilt angles, both magnetic flux and fluid are expelled from regions of strong vorticity, consistent with observations in the outer heliosphere at solar minimum at times when the north-south oscillations are present. Well-defined corotating interaction regions form throughout the entire radial domain. These are characterized by regions of positive correlation between B and ρ. Beyond 20 AU, where the north-south oscillations are observed, pickup ions should have increased the temperature and pressure of the interaction regions and caused them to both expand and damp, a process we cannot at present model. In future work we will explore these three-dimensional effects in time-dependent compressible MHD for supersonic velocity jumps.

Acknowledgments. This research was supported by a Supporting Research and Technology grant at the NASA Goddard Space Flight Center. M.L.G. and D.A.R. acknowledge stimulating discussions with A. Usmanov and P. Cargill.

Janet G. Luhmann thanks the three referees for their assistance in evaluating this paper.

References

Boris, J.P., and D.L. Book, Flux corrected transport, I, SHASTA A fluid transport algorithm that works, *J. Comput. Phys., 11*, 38, 1973.

Burlaga, L.F., A heliospheric vortex street?, *J. Geophys. Res., 95*, 4333, 1990.

Burlaga, L.F., and N.F. Ness, Radial and latitudinal variations of the magnetic field strength in the outer heliosphere, *J. Geophys. Res., 98*, 3539, 1993.

Burlaga, L.F., and J.D. Richardson, North-south flows at 47 AU: A heliospheric vortex street?, *J. Geophys. Res., 105*, 10,501, 2000.

Burlaga, L.F., N.F. Ness, and J.W. Belcher, Radial evolution of corotating merged interaction regions and flows between $\approx$ 14 AU and $\approx$ 43 AU, *J. Geophys. Res., 102 (A3)*, 4661-4672, 1997.

Cargill, P.J., J. Schmidt, D.S. Spicer, and S.T. Zalesak, Magnetic structure of overexpanding coronal mass ejections: Numerical models, *J. Geophys. Res., 105*, 7509, 2000.

DeVore, C.R., Flux-corrected transport techniques for multidimensional compressible magnetohydrodynamics, *J. Comput. Phys., 92*, 142, 1991.

Goldstein, M.L., D.A. Roberts, A.E. Deane, S. Ghosh, and H.K. Wong, Numerical simulation of Alfvénic turbulence in the solar wind, *J. Geophys. Res., 104,* 14, 1999.

Korzhov, N.P., V.V. Mishin, and V.M. Tomozov, On the role of plasma parameters and the Kelvin-Helmholtz instability in a viscous interaction of solar wind streams, *Planet. Space. Sci., 32,* 1169, 1984.

Lamb, S.H., *Hydrodynamics,* 224 pp., Dover, Mineola, N. Y., 1945.

Lazarus, A.J., B. Yedidia, L. Villanueva, and R.L. McNutt, Meridional plasma flow in the outer heliosphere, *Geophys. Res. Lett., 15,* 1519, 1988.

McNutt, R., Possible explanations of north-south plasma flow in the outer heliosphere and meridional transport of magnetic flux, *Geophys. Res. Lett., 15,* 1523, 1988.

Odstrcil, D. and V.J. Pizzo, Simulations of the Kelvin-Helmholtz instability in the outer heliosphere, *Eos Trans. AGU, 78*(46) Fall Meet. Suppl. F530, 1997.

Parker, E.N., *Interplanetary Dynamical Processes,* Wiley-Interscience, New York, 1963.

Parker, E.N., Dynamical properties of solar and stellar winds, III, *Astrophys. J., 139,* 690, 1964.

Pizzo, V., A three-dimensional model of corotating streams in the solar wind, 3, Magnetohydrodynamic streams, *J. Geophys. Res., 87,* 4374, 1982.

Pizzo, V., Global, quasi-steady dynamics of the distant solar wind, 1, Origin of north-south flows in the outer heliosphere, *J. Geophys. Res., 99,* 4173, 1994.

Pizzo, V.J., and B.E. Goldstein, Meridional transport of magnetic flux in the solar wind between 1 AU and 10 AU: A theoretical analysis, *J. Geophys. Res., 92,* 7241, 1987.

Pizzo, V.J., D.S. Intriligator, and G.L. Siscoe, Radial alignment simulation of solar wind streams observed by Pioneers 10 and 11 in 1974, *J. Geophys. Res., 100,* 12,251, 1995.

Richardson, J.D., K.I. Paularena, and C. Wang, The solar wind in the outer heliosphere, *Solar Wind Nine,* edited by S.R. Habbal et al., 183-188, *AIP Conf. Proc., 471,* 1999.

Roberts, D.A., M.L. Goldstein, and L.W. Klein, The amplitudes of interplanetary fluctuations: Stream structure, heliocentric distance, and frequency dependence, *J. Geophys. Res., 95,* 4203, 1990.

Siregar, E., D.A. Roberts, and M.L. Goldstein, An evolving MHD vortex street model for quasi-periodic solar wind fluctuations, *Geophys. Res. Lett., 19,* 1427, 1992.

Siregar, E., D.A. Roberts, and M.L. Goldstein, Quasi-periodic transverse plasma flow associated with an evolving MHD vortex street in the outer heliosphere, *J. Geophys. Res., 98,* 13,233, 1993.

Siregar, E., W.T. Stribling, and M.L. Goldstein, On the dynamics of a plasma vortex street and its topological signatures, *Phys. Plasmas, 1,* 2125, 1994.

Siscoe, G., and D. Intriligator, Three views of two giant streams: Aligned observations at 1 AU, 4.6 AU, and 5.9 AU, *Geophys. Res. Lett., 20,* 2267, 1993. (Correction, *Geophys. Res. Lett., 21,* 2861, 1994.)

Slavin, J.A., E.J. Smith, and B.T. Thomas, Large scale temporal and radial gradients in the IMF: Helios 1, 2, ISEE-3, and Pioneer 10, 11, *Geophys. Res. Lett., 11,* 279, 1984.

Totten, T. L., J. W. Freeman, and S. Arya, An empirical determination of the polytropic index for the free-streaming solar wind using Helios 1 data, *J. Geophys. Res., 100,* 13, 1995.

Triskova, L., P. Sroubek, and I.S. Veselovskij, On vortex flow structures in the outer heliosphere, *Stud. Geophys. Geod., 36,* 57, 1992.

Veselovsky, I.S., Solar wind vortex flow in the outer heliosphere, in *Physics of the Outer Heliosphere,* edited by S. Grzedzielski and D.E. Page, p. 277, Pergamon, Tarrytown, N. Y., 1990.

Veselovsky, I.S., and L. Triskova, MHD spiral vortex tubes of the solar wind in the outer heliosphere, *Stud. Geophys. Geod., 34,* 362, 1990.

Winterhalter, D., and E.J. Smith, Observations of large scale spatial gradients in the heliospheric magnetic field, *Adv. Space Res., 9*(4), 171, 1989.

Zalesak, S.T., Fully multidimensional flux-corrected transport algorithms for fluids, *J. Comput. Phys., 31,* 335, 1979.

L. F. Burlaga, M. L. Goldstein, D. A. Roberts, and E. Siregar, NASA Goddard Space Flight Center, Code 692, Greenbelt, MD 20771. (burlaga@lepvax.gsfc.nasa.gov; melvyn.goldstein@gsfc.nasa.gov; roberts@vayu.gsfc.nasa.gov; yses@puff.gsfc.nasa.gov)

A. E. Deane, Institute for Physical Science and Technology, University of Maryland, College Park, MD 20742.

April 27, 2000; revised September 28, 2000; accepted October 12, 2000.